Journal of Quantitative Spectroscopy & Radiative Transfer 112 (2011) 1050–1064

Contents lists available at ScienceDirect

Journal of Quantitative Spectroscopy & Radiative Transfer

journal homepage: www.elsevier.com/locate/jqsrt

Validation of the community radiative transfer model

Shouguo Ding [a], Ping Yang [a,*], Fuzhong Weng [b], Quanhua Liu [c,d], Yong Han [b], Paul van Delst [d], Jun Li [e], Bryan Baum [f]

[a] Department of Atmospheric Sciences, Texas A&M University, College Station, TX 77843, USA
[b] Satellite Meteorology and Climatology Division, Center for Satellite Applications and Research, NOAA/NESDIS, Camp Springs, MD 20746, USA
[c] QSS Group, Incorporated, Camp Springs, MD 20746, USA
[d] Joint Center for Satellite Data Assimilation, NOAA/NESDIS, Camp Springs, MD 20746, USA
[e] Cooperative Institute for Meteorological Satellite Studies, University of Wisconsin-Madison, Madison, WI 53706, USA
[f] Space Science and Engineering Center, University of Wisconsin Madison, Madison, WI 53706, USA

ARTICLE INFO

Article history:
Received 1 April 2010
Received in revised form
5 November 2010
Accepted 10 November 2010
Available online 13 November 2010

Keywords:
Validation
CRTM
DISORT
LBLRTM
AIRS
IASI
ECMWF

ABSTRACT

To validate the Community Radiative Transfer Model (CRTM) developed by the U.S. Joint Center for Satellite Data Assimilation (JCSDA), the discrete ordinate radiative transfer (DISORT) model and the line-by-line radiative transfer model (LBLRTM) are combined in order to provide a reference benchmark. Compared with the benchmark, the CRTM appears quite accurate for both clear sky and ice cloud radiance simulations with RMS errors below 0.2 K, except for clouds with small ice particles. In a computer CPU run time comparison, the CRTM is faster than DISORT by approximately two orders of magnitude. Using the operational MODIS cloud products and the European Center for Medium-range Weather Forecasting (ECMWF) atmospheric profiles as an input, the CRTM is employed to simulate the Atmospheric Infrared Sounder (AIRS) radiances. The CRTM simulations are shown to be in reasonably close agreement with the AIRS measurements (the discrepancies are within 2 K in terms of brightness temperature difference). Furthermore, the impact of uncertainties in the input cloud properties and atmospheric profiles on the CRTM simulations has been assessed. The CRTM-based brightness temperatures (BTs) at the top of the atmosphere (TOA), for both thin ($\tau < 5$) and thick ($\tau > 30$) clouds, are highly sensitive to uncertainties in atmospheric temperature and cloud top pressure. However, for an optically thick cloud, the CRTM-based BTs are not sensitive to the uncertainties of cloud optical thickness, effective particle size, and atmospheric humidity profiles. On the contrary, the uncertainties of the CRTM-based TOA BTs resulting from effective particle size and optical thickness are not negligible in an optically thin cloud.

1. Introduction

Satellite-based observations across the visible, infrared, and microwave spectral regions provide valuable information on clouds, which cover, on an average, approximately 70% of the globe. However, most satellite measurement assimilation approaches have focused on satellite data for clear-sky conditions [1]. Since clouds are dominant in regions undergoing quickly changing weather conditions, a rational and computationally efficient method to use satellite cloud information is needed. Numerical weather prediction (NWP) models could use such a method to enhance the simulation and forecasting capabilities under both clear and cloudy conditions [2–6]. To include cloudy conditions, satellite radiance data assimilation must have an efficient and accurate forward radiative transfer model to handle water and ice cloud particle absorption and multiple radiation scattering. The development of the Community Radiative Transfer Model (CRTM) and its subsequent improvements have created a better method

* Corresponding author.
E-mail address: pyang@tamu.edu (P. Yang).

0022-4073/$ - see front matter © 2010 Elsevier Ltd. All rights reserved.
doi:10.1016/j.jqsrt.2010.11.009

for NWP models to assimilate satellite measurements made under all weather conditions.

The CRTM was developed by the U.S. Joint Center for Satellite Data Assimilation (JCSDA) to provide fast, accurate satellite radiance simulations and Jacobian calculations at the top of the atmosphere (TOA) under all weather and surface conditions [7]. The model has undergone substantial improvement and expansion, since the first version was released in 2004. The CRTM has been used in the NOAA/NCEP data assimilation system for supporting weather forecasting, in the NOAA/NCEP and the National Aeronautics and Space Administration (NASA) Global Modeling and Assimilation Office (GMAO) reanalysis, and in other satellite-based radiance data applications [8]. The CRTM supports the simulation of sensor measurements covering wavelengths ranging from the visible through the microwave.

The infrared (IR) high spectral resolution sounder whose measurements can be simulated by the CRTM has attracted significant attention. High spectral resolution measurements are used to derive vertical profiles of atmospheric temperature, water vapor, trace gases, such as ozone and methane, cloud properties such as cloud top pressure, and Earth surface properties. The atmospheric soundings are produced at higher vertical resolutions and with greater accuracy than those from broadband sounders, such as the High Resolution Infrared Radiometer Sounder (HIRS) and the Geostationary Operational Environmental Satellite (GOES) Sounder. The operation of the Atmospheric Infrared Sounder (AIRS) [9] and the Infrared Atmospheric Sounding Interferometer (IASI) [10], aboard the Aqua and MetOp polar orbiting satellites, respectively, has proved successful. These high spectral resolution IR sounders have thousands of channels with spectral widths narrower than one wavenumber. The spectrally resolved radiance data observed by AIRS and IASI contains a wealth of information about the atmosphere and the Earth's surface and provides an unprecedented opportunity to significantly advance our knowledge of the earth–atmosphere system. The accurate vertical sounding information is important for nowcasting, NWP, and many other applications. Recent studies have demonstrated the high spectral resolution IR sensors can be used to monitor low-level atmospheric activities and to substantially enhance the forecasting of mesoscale and regional severe weather events, including tropical storms and hurricanes [11–13].

The availability of the products based on AIRS and IASI observations with collocated MODIS and other cloud products provide an opportunity to validate the CRTM. The intent of the present study is to provide an assessment of the CRTM simulation of high spectral resolution capabilities for ice cloud scenarios and to improve the model based on a better understanding of the physics involved.

Two approaches are used to validate the CRTM-based high spectral brightness temperatures. The first approach, the model-to-model method, is a rigorous model based on a combination of the Line-By-Line Radiative Transfer Model (LBLRTM) [14] and the Discrete Ordinate Radiative Transfer (DISORT) [15] model and was developed to provide reference simulations under both clear sky and ice cloud conditions. Subsequently, the brightness temperatures (BTs) from the reference model are compared to the CRTM-based, with IASI spectral resolution, upwelling spectral BTs at the TOA. The sensitivity of the simulated BTs to the ice cloud macrophysical and microphysical properties is investigated. In the second approach, the CRTM simulations are compared directly with AIRS observations.

We have organized the paper into six sections. Section 2 briefly describes the three radiative transfer models used in this study: CRTM, LBLRTM, and DISORT. The single-scattering properties of ice clouds are discussed in Section 3. In Section 4, we compare the simulated high spectral brightness temperatures from the reference model (LBLRTM+DISORT) with the CRTM, and further investigate the sensitivity of brightness temperatures to cloud macrophysical and microphysical properties. In Section 5, the simulated radiances from the CRTM, using the operational MODIS cloud products and the ECMWF atmospheric profiles, are compared with those measured from an AIRS. A summary discussion is given in Section 6.

2. Data and models

2.1. The community radiative transfer model (CRTM)

The CRTM is a state-of-the-art satellite radiance simulator including both a forward model, which simulates the upwelling radiances for a given sensor, and its Jacobian, which calculates the radiance derivatives with respect to the input atmospheric state variables [7]. Under all atmospheric and surface conditions [5], the CRTM is capable of accounting for the absorption of atmospheric gases as well as the multiple scattering of water clouds, of ice clouds composed of a variety of nonspherical habits, and of a variety of aerosols. To be more specific, the CRTM includes four major modules to handle atmospheric transmittance, surface properties including albedo and emissivity, cloud and aerosol optical properties and radiative transfer [5]. The atmospheric transmittance module uses a fast model, the Optical Path TRANsmittance (OPTRAN) model, to compute the gaseous absorption for the given pressure, temperature, water vapor, and ozone concentration profiles [7]. The surface emissivity/reflectivity module consists of ocean, land, snow, and ice surface components and is further divided into smaller modules according to the spectral region and surface sub-type. In the cloud/aerosol module, six cloud and eight aerosol types are included with pre-computed optical property lookup tables (LUTs). The cloud/aerosol module includes: water and rain cloud types; ice, graupel, snow, and hail cloud types defined by their cloud particle densities: 0.9, 0.4, 0.1, and 0.9 g cm^{-3}; and, the aerosol types of dust, dry organic carbon (OC), wet OC, dry black carbon (BC), wet BC, sea salt accumulation mode (SSAM), sea salt coarse mode (SSCM), and sulfate. The cloud/aerosol module can be used for multiple cloud/aerosol layers in a vertical column [5]. The advanced fast doubling–adding method, described in detail by Liu and Weng [16], is used in the radiative transfer module to solve the radiative transfer equation.

2.2. LBLRTM+DISORT model

Accurate simulations of thermal IR radiances at the TOA must account for the gaseous absorption in the

atmosphere. In the IR window region, the gaseous absorption is especially important for optically thin clouds. To investigate the performance of the CRTM under semi-transparent ice cloud conditions, we have established a rigorous reference model by combining the Line-By-Line Radiative Transfer Model (LBLRTM) [14] and the Discrete Ordinate Radiative Transfer (DISORT) model [15] (henceforth LBLRTM+DISORT). The LBLRTM, developed by the Atmospheric and Environmental Research Inc. (the computer code available at http://www.rtweb.aer.com/), is an accurate and flexible radiative transfer model (RTM) for gaseous absorption and emission over the full spectral range from the ultra-violet to microwave. The LBLRTM is regarded as a standard benchmark for the computation of gaseous absorption and emission in vertically inhomogeneous atmospheres.

The main attributes of LBLRTM can be summarized [17]: (1) the application of the Voigt line shape with a line cutoff at 25 cm^{-1} from line center to all lines at all layers; (2) the incorporation of the continuum model MT_CKD, which includes both self-broadened and foreign-broadened water vapor; and (3) the inclusion of continuum absorption of carbon dioxide, oxygen, nitrogen, and ozone and of an extinction due to Rayleigh scattering. The algorithmic accuracy of an LBLRTM is roughly 0.5% and the limiting errors are due to the line parameters and the line shape. The LBLRTM has been extensively used in the development of fast radiative transfer models. For example, the OPTRAN and Optimal Spectral Sampling (OSS) [18] models are trained using LBLRTM in the infrared region. In this study, version LBLRTM_v11.6, with high spectral resolution, is used to calculate the gaseous optical thickness profile for a given atmospheric pressure, temperature, water vapor, and ozone concentration.

DISORT is based on the discrete ordinates method [15,19] and calculates the multiple scattering of a vertically inhomogeneous non-isothermal plane-parallel atmosphere, when given the values of optical thickness, single-scattering albedo, and the scattering phase function for the scattering/absorbing medium of any specific atmospheric layer. DISORT provides a comparison standard for other modeling results and is important for larger models such as MODTRAN [20] and SBDART [21]. This study is based on the publicly available and most current version of the DISORT code, DISORT 2.0 beta. The scattering phase function is specified in terms of Legendre polynomial expansion coefficients. To accurately represent the full original scattering phase function, thousands of Legendre polynomial terms are required for a phase function with a strong forward peak. One way to reduce the number of necessary Legendre terms is to truncate the forward scattering peak and renormalize the phase function. By truncating the forward peak and renormalizing the phase function, less than 100 terms are needed to replicate the phase function and to significantly reduce the computational time, which is proportional to the third power of the number of radiation streams. Two techniques have been developed to represent the scattering phase function in terms of Legendre polynomials in radiative transfer simulations: the δ–M method by Wiscombe [22] and the δ-fit method by Hu et al. [23]. In this study, the δ-fit method is used to truncate the strong forward peak of the phase function associated with large ice particles [24].

To truncate the forward peak of the scattering phase function, optical thickness, and single-scattering albedo adjustments must be made [25] to account for the forward peak energy. The adjusted optical thickness and single-scattering albedo can be expressed by

$$\tau' = (1-f\omega)\tau \tag{1}$$

$$\omega' = \frac{(1-f)\omega}{1-f\omega} \tag{2}$$

where f is the portion of the scattered energy associated with the truncated forward peak, τ and ω are the original optical thickness and single-scattering albedo, and τ' and ω' are the adjusted optical thickness and single-scattering albedo associated with the truncated phase function.

2.3. Infrared atmospheric sounding interferometer (IASI)

An IASI is a downward-view sounding instrument for the measurement of high-resolution atmospheric temperature, water vapor, and other trace gas profiles. The first IASI was launched on the MetOp-A satellite on 19 October 2006. The instrument has 8461 channels, assembled in three bands, between 645.0 and 2760 cm^{-1} (15.5 and 3.63 μm) with a spectral resolution of 0.5 cm^{-1} and a ground spatial resolution of 12 km at nadir.

2.4. Infrared atmospheric sounder (AIRS)

Similar to IASI, AIRS, onboard the NASA Earth Observing System (EOS) Aqua satellite launched on 4 May 2002, is a high spectral resolution ($v/\Delta v$=1200) IR sounder with 2378 channels. AIRS radiances in the IR wavelength region of 3.74–15.4 μm (649.5–2665.0 cm^{-1}) enable the retrieval of the vertical profiles of atmospheric temperature and water vapor from the Earth's surface to an altitude of 40 km with a horizontal resolution of 13.5 km at nadir.

3. Bulk scattering properties of ice particles

Ice clouds are composed of particles with a variety of sizes and complex shapes (or habits) that depend on the temperature, humidity, and local dynamic conditions of the environment. The scattering properties are highly sensitive to ice particle habits. Since ice habits are as varied as snowflakes, the most common practice is to focus on a small set of habits to represent those occurring in ice clouds. Extensive libraries of the single-scattering properties of ice particles for six habits (droxtals, hexagonal plates, hollow columns, solid columns, three-dimensional bullet rosettes, and aggregates) have been generated by a combination of the improved geometric optics method (IGOM) and the finite difference time domain method (FDTD) [26–28]. In the CRTM, the single-scattering properties of individual habits are computed at 65 wavelengths ranging 0.2–100 μm and for 45 size bins based on particle maximum diameters ranging 2–9500 μm.

Since the single-scattering properties of individual particles are insufficient to represent ice clouds with both

particle size and habit distributions, the ice cloud bulk scattering properties are required. The bulk scattering properties of ice clouds are calculated by integrating the single-scattering properties of individual ice particles over a given set of particle size and habit distributions. Here, we use a set of 1117 particle size distributions obtained from in situ measurement experiments made during various field campaigns in both tropical and mid-latitude regions [29–32]. Each particle size distribution (PSD) is parameterized in terms of the gamma distribution in the form

$$n(D) = N_0 D^u e^{-\lambda D}, \tag{3}$$

where $n(D)$ is the particle concentration per unit volume, N_0 is the intercept, λ is the slope, μ is the dispersion, and D is the maximum size of the ice particle.

Different ice cloud habit distributions have been used to infer cloud scattering properties [25,29–33]. In this study, we chose a habit mixture scheme used in the MODIS Collection 5 operational products [29–31]: $D \le 60$ μm—100% droxtals; $60 < D \le 1000$ μm—15% 3D bullet rosettes, 50% solid columns, and 35% hexagonal plates; $1000 < D \le 2500$ μm—45% hollow columns, 45% solid columns, and 10% aggregates; and, $D > 2500$ μm—97% 3-D bullet rosettes and 3% aggregates. The bulk scattering properties are functions of particle effective size and wavelength and include the extinction efficiency Q_{ext}, single-scattering albedo ω, asymmetry factor g, and scattering phase function $P(\Theta)$, where Θ is the scattering angle. Fig. 1 shows the scattering phase functions of ice clouds with various effective sizes at wavelengths of 8.5 and 12.0 μm. Fig. 2 shows the ice cloud bulk scattering properties as functions of wavenumber and effective particle size with the single-scattering albedo on the left and the extinction efficiency on the right.

4. Model comparison and sensitivity study

The CRTM simulated, upwelling IR high spectral BTs at the TOA are compared with those from the LBLRTM+DISORT for both clear sky and ice cloud conditions. In addition, the influence of the assumed ice cloud macro- and microphysical properties on the simulated high-spectral-resolution BTs at TOA is explored. Recent sensitivity studies illuminate the effect of cloud properties, including cloud optical thickness and effective particle size, on the simulation of radiances for the solar region [34–36]. The influence of cloud geometric thickness on the retrieval of cloud optical thickness and effective particle size is much

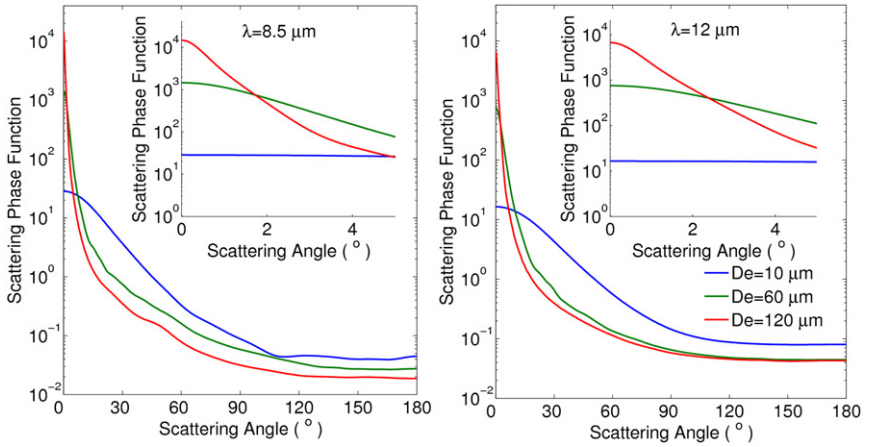

Fig. 1. Scattering phase functions of ice clouds with various effective particle sizes at wavelengths of 8.5 and 12.0 μm.

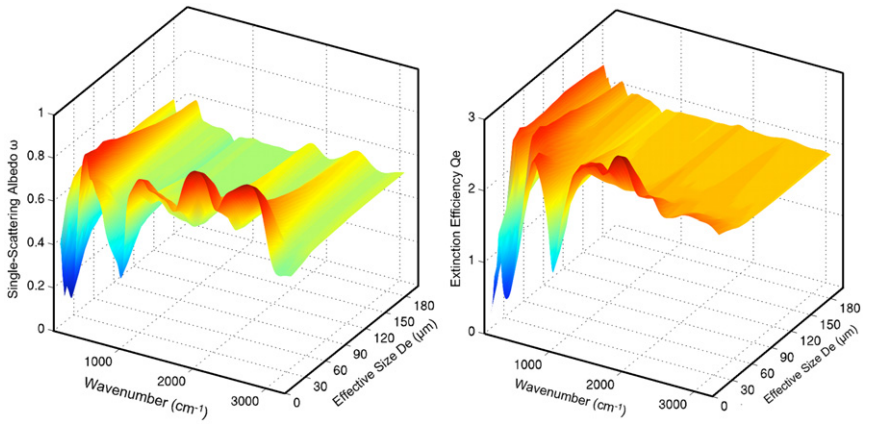

Fig. 2. Variation of ice cloud single-scattering albedo (left), and extinction efficiency (right) with wavenumber and effective particle size.

larger for IR retrievals than for the solar-band-based algorithm [37–39]. These studies also demonstrate the importance of the surface and atmospheric temperatures, trace gas profiles, and cloud properties for simulating the upwelling IR spectrum BTs at the TOA.

To investigate the sensitivity of the IR high-spectral-resolution BT to the ice cloud optical, macro- and microphysical properties, the simulations are performed for the IASI spectrum, specifically, IASI band 1 (645–1210 cm^{-1}). The McClatchey tropical standard atmospheric vertical profiles [40] of pressure, temperature, water vapor, and ozone are used in the simulations with both the CRTM and LBLRTM+DISORT. The atmospheric profile is interpolated into 100 fixed layers from the surface to 100 km and with a vertical resolution of 0.5 km below 30 km. The surface temperature is assumed to be 300.0 K. For the LBLRTM+DISORT model, an LBLRTM provides the gaseous absorption optical thickness of each atmospheric layer.

For clear sky cases, DISORT directly calculates the upwelling radiances without considering multiple scattering. For ice cloud simulations, DISORT additionally requires the appropriate single-scattering cloud properties of each cloudy layer to calculate multiple scattering. The ice cloud bulk scattering properties used for the radiance simulations in the LBLRTM+DISORT coupled model are the same as those used in the latest version of the CRTM. The high spectral bulk scattering properties of an ice cloud with the IASI spectral resolution are derived from interpolating the bulk scattering library to the center wavenumber of each channel. The scattering phase functions of each IASI channel are normalized after using the logarithmic interpolation method. For single-scattering albedo, extinction efficiency, and other parameters, a linear interpolation method was found to be sufficient.

In previous studies, AIRS data were analyzed to infer cloud optical thickness and effective particle size [38,39].

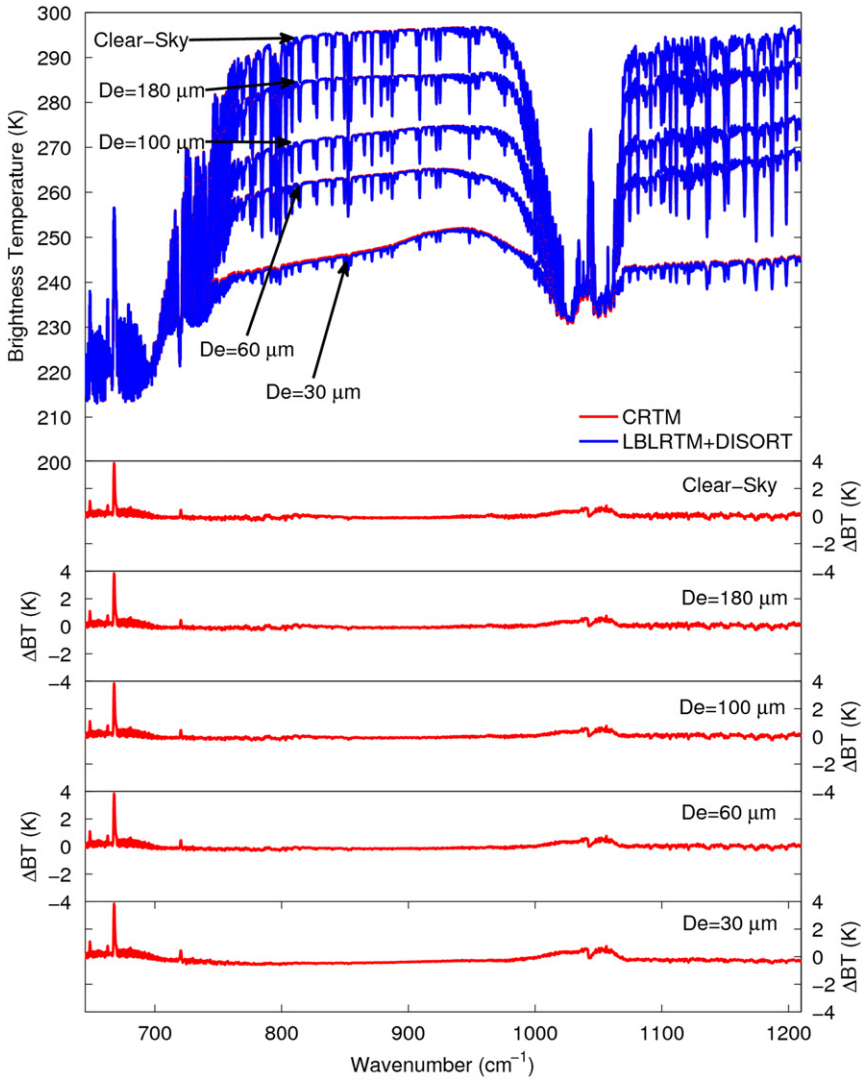

Fig. 3. Comparison of an IASI band 1 brightness temperatures (BTs) simulated from the CRTM forward model and the LBLRTM+DISORT model for clear-sky and ice cloud cases. The ice water path (IWP) for the ice cloud layers is assumed to be 0.02 kg m^{-2}. Effective particle sizes are 30, 60, 100, and 180 μm. Surface and cloud-top temperatures are 300 and 232 K.

The optical thickness and particle size provide the ice water path (IWP). One can also develop a parameterization to infer optical thickness as a function of IWP and effective particle size. In the CRTM, the ice cloud IWP is specified. To simplify the comparisons between the CRTM and LBLRTM+DISORT simulations, a single-layered ice cloud is specified with a constant IWP, 0.02 kg m^{-2}, located between 9.0 and 10.0 km above the surface. The cloud top and cloud base temperatures are 232.0 and 240.5 K, respectively. The various ice particle effective size values are assumed to be 30, 60, 100, and 180 μm. The high-spectral-resolution IR BTs of an IASI band 1 at TOA are simulated from LBLRTM+DISORT at nadir (i.e., viewing the zenith angle $\theta=0^{\circ}$). Analogous simulations were performed by the CRTM with the same set of input data. The difference of spectral brightness temperatures (ΔBT) between the CRTM and LBLRTM+DISORT is defined as follows:

$$\Delta BT = BT_{CRTM} - BT_{DISORT} \quad (4)$$

Similar to the previous studies [41,42], the root mean square (RMS) errors are used as an index for the overall

Table 1
RMS values of each spectral ΔBT from the CRTM to DISORT.

	De=30 μm	De=60 μm	De=100 μm	De=180 μm	Clear sky
RMS of ΔBT (K)	0.3490	0.1816	0.1668	0.1660	0.1619

Table 2
Comparison of CPU time between CRTM and DISORT on a Dual 2.6 GHz 64-bit AMD computer.

	Clear sky (s)	Cloudy (s)
CRTM	1.66	3.95
DISORT	375.62	542.70

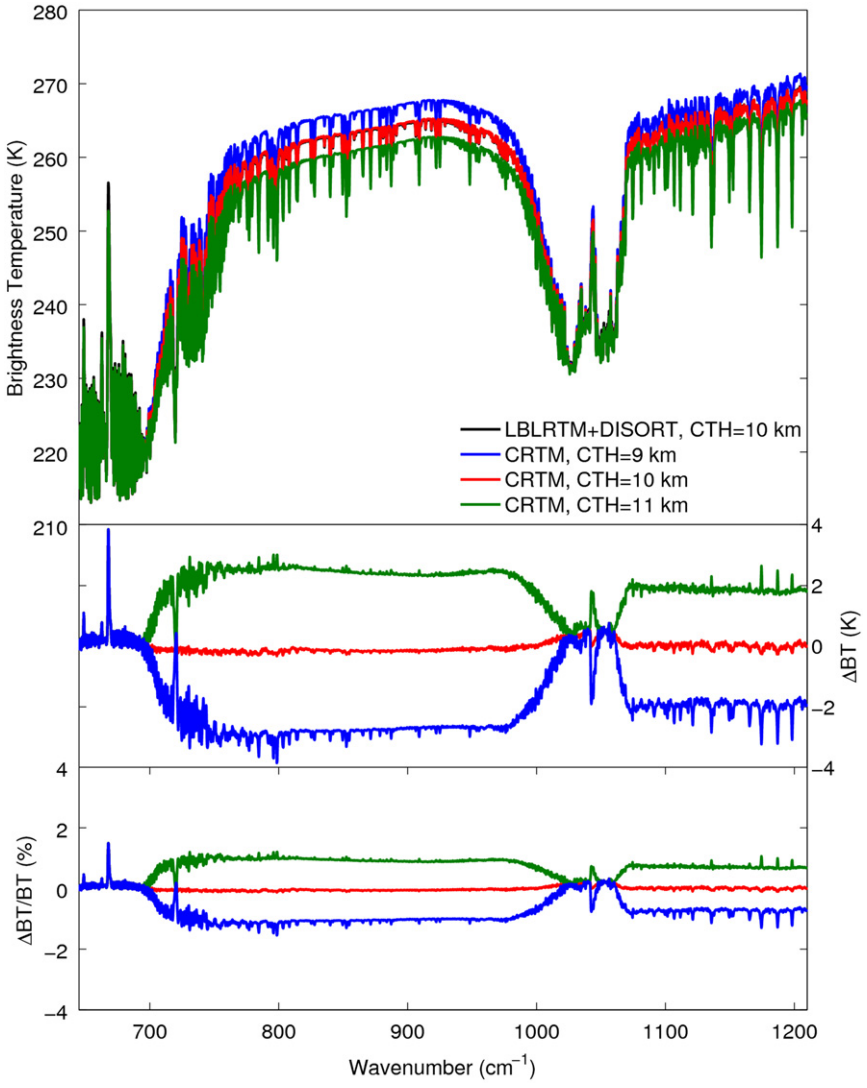

Fig. 4. CRTM simulated brightness temperatures and their relative changes with respect to a reference from LBLRTM+DISORT, for a cloud geometrical thickness of 1 km. Cloud IWP is fixed to 0.02 kg m^{-2} and cloud top height varies from 9 to 11 km with a 1-km interval.

error level of the CRTM and are provided in terms of the ΔBT, when compared with the LBLRTM+DISORT model. The RMS error is defined as the square root of the arithmetic mean of the squares of a set of spectral ΔBTs and can be given by

$$RMS(\Delta BT) = \sqrt{\frac{\sum_{i}^{N} (\Delta BT_i)^2}{N}}, \quad (5)$$

where N is the total number of spectral points and ΔBT_i is the difference of BT between the CRTM and LBLRTM+DISORT models at the ith channel. The Noise Equivalent Differential Temperature (NEDT) of current hyperspectral IR sounders, such as AIRS and IASI, are at the level of 0.2 K [43,44]. According to the accuracy estimation and error analysis based on two fast infrared radiative transfer models reported by Niu et al. [41] and Zhang et al. [42], the typical error level is in the order of 0.5 K. In view of these facts, an acceptable error level for the CRTM under ice cloud conditions should be about the same as the NEDT or lower than 0.5 K.

Fig. 3 shows the results of simulated upwelling high-spectral-resolution brightness temperatures in an IASI band 1 at TOA from both models under clear sky and ice cloud conditions. Strong gaseous absorption in the 15 μm CO_2 band and the 9.6 μm O_3 band is evident for both clear-sky and cloudy conditions. For the clear-sky case, the differences between the two models are < 0.2 K, except at some wavenumbers near 670 cm^{-1} (15.0 μm CO_2 band) and 1040 cm^{-1} (9.6 μm O_3 band), which indicates the CRTM is quite accurate for clear-sky radiance simulations. The RMS values of each spectral ΔBT in Fig. 3 are listed in Table 1. As shown in Table 1, the errors decrease with an increase in ice particle effective size. The largest error, 0.349 K, occurs when D_e=30 μm, but is still less than 0.5 K.

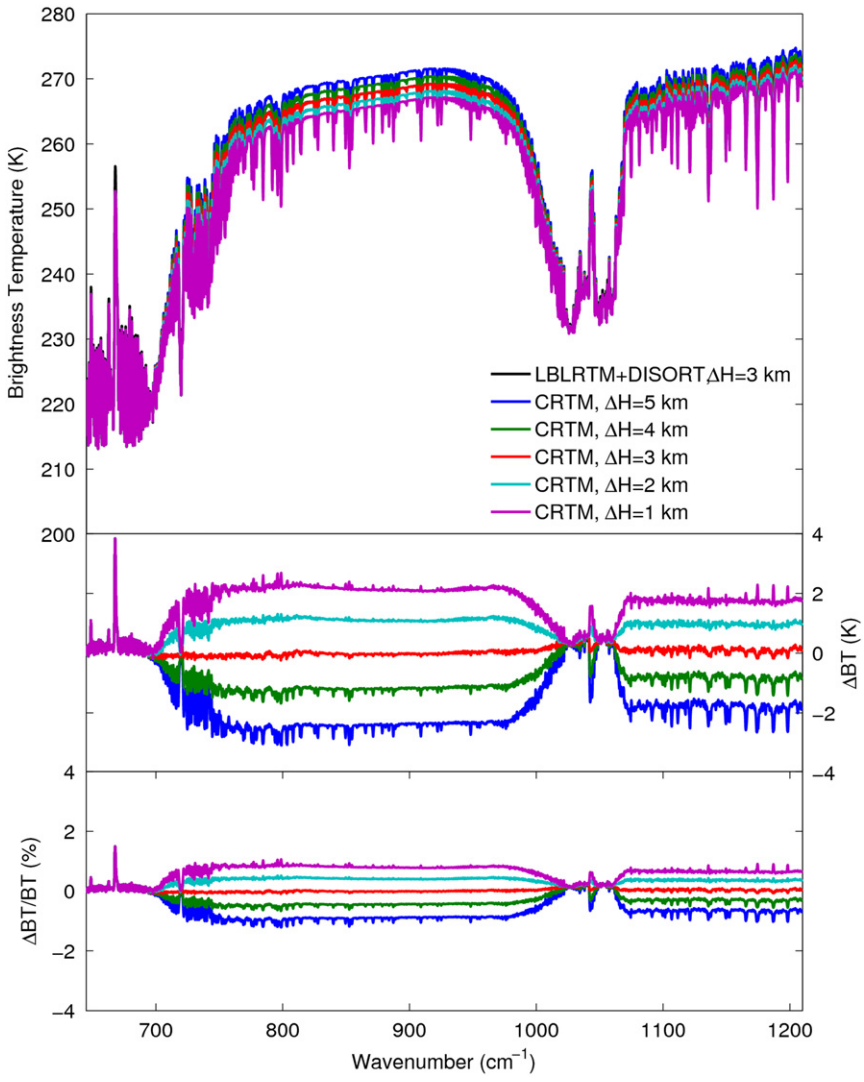

Fig. 5. CRTM simulated brightness temperatures and their relative changes with respect to a reference from LBLRTM+DISORT for a cloud geometrical thickness of 3.0 km. Cloud IWP is fixed at 0.02 kg m^{-2} and cloud geometrical thickness varies from 1 to 5 km with an interval of 1 km.

The results in Fig. 3 indicate that the TOA BTs within the window region are sensitive to a range of effective particle sizes, except in bands of strong gaseous absorption. The spectral BTs increase with wavenumber, and the slopes in BTs as a function of particle size within the 750–950 cm^{-1} region agree with the previous findings [37,38].

The computational efficiency is compared for the two models in Table 2, which lists the CPU time required by the CRTM and by the LBLRTM+DISORT model for both clear-sky and ice cloud cases on a computer with a dual processor 2.6 GHz 64-bit AMD Opteron system. For the clear-sky case, the CRTM is approximately 226 times more efficient than the LBLRTM+DISORT model.

Fig. 4 illustrates the influence of cloud top height on the simulated BTs in an IASI band 1 for a single-layered ice cloud with a constant IWP of 0.02 kg m^{-2}, given the same atmospheric profiles and surface temperatures as in Fig. 2. For these simulations, the cloud top height is 9, 10 or 11 km, the cloud particle effective size is 60 μm, and the cloud geometric thickness is 1 km. The reference simulation from LBLRTM+DISORT is provided for a cloud top height of 10 km. As shown in Fig. 4, the ΔBTs simulated for an IASI band 1 between the two models for the reference cloud top height, 10 km, are relatively small. In this case, the absolute values of ΔBT are larger than 2 K and the corresponding relative changes of ΔBT/BT are on the order of 1%, as cloud top height varies from 9 to 11 km in the window region, except for the strongly absorbing CO_2 and O_3 bands. Overall, the results in Fig. 4 show the upwelling brightness temperatures at the TOA are sensitive to the cloud top height.

The effects of the cloud geometric thickness on the simulated upwelling BTs of an IASI band 1 are investigated in the same way as for the cloud top height. In this case, the cloud particle effective size and cloud top height are fixed at 60 μm and 10 km, respectively, while the cloud geometric thickness varies from 1 to 5 km in 1 km intervals. The simulated spectral BTs from the CRTM are shown in Fig. 5. For comparison, a reference simulation from LBLRTM+DISORT with an assumed 3 km cloud geometric thickness is used. The ΔBTs and the relative changes in BTs (ΔBT/BT) with respect to the simulations from LBLRTM+DISORT are also shown in Fig. 5. The absolute values of ΔBT and the relative changes of ΔBT/BT increase with increasing differences in the cloud geometric thickness. Similar to the results shown in Fig. 4, the influence on the spectral BTs increases with the difference in cloud geometric thickness. The absolute values of ΔBT are about 1 K per kilometer of the cloud geometric thickness and the corresponding relative changes of ΔBT/BT are on the order of 0.5% per kilometer of the cloud geometric thickness in the window region, except for the CO_2 and O_3 bands. Based on the results shown in Figs. 4 and 5, the influence of the cloud top height on the spectral BTs is approximately two times greater than that of the cloud geometric thickness when both changes have the same 1 km value. Although the variations in cloud geometric thickness have less influence on simulated upwelling BTs than variations in the cloud top height, uncertainties in the cloud geometric thickness are not negligible in the cloud radiative transfer calculations.

5. Comparison with AIRS radiance observations

Since MODIS and AIRS are both on NASA's EOS Aqua platform, the instruments almost simultaneously view the same ground location. Collocation between MODIS and AIRS measurements has spurred numerous studies [11,45–48]. In this section, the spectral BTs at the TOA simulated from CRTM, with collocated ECMWF data products and MODIS cloud products as an input, are compared with those of collocated AIRS observations. Specifically, the input ice cloud parameters data (optical thickness, effective radius, and cloud top pressure (CTP)) for the CRTM forward model are obtained from the operational MODIS cloud product (MYD06 Collection 5), and the atmospheric temperature and humidity profiles are derived from the collocated ECMWF analysis data. Fig. 6 is a flowchart outlining the comparison procedure.

A number of standard MODIS operational atmospheric parameter data products are available [49]. The MYD06

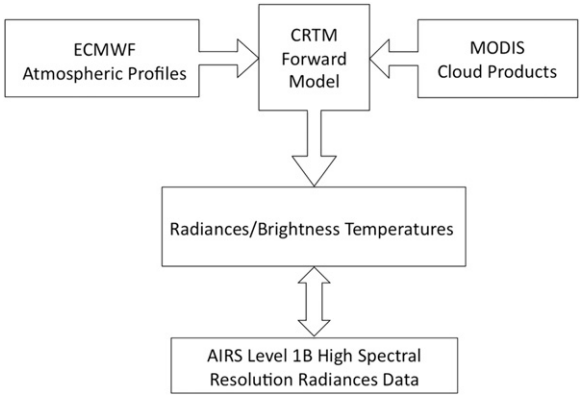

Fig. 6. Flowchart outlining the validation of the CRTM using MODIS cloud products and ECMWF atmospheric profiles and AIRS high-spectral-resolution radiance data.

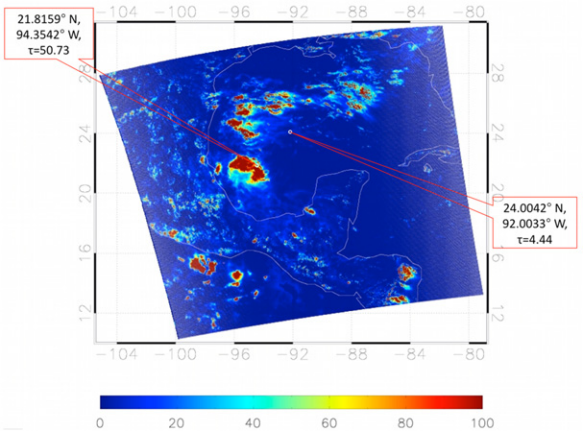

Fig. 7. Ice cloud optical thickness derived from a MODIS granule taken over the Gulf of Mexico on 7 September 2009 at 19:30 UTC. Two selected MODIS pixels in the presence of ice clouds: one for an optically thick cloud (τ=50.73) and latitude and longitude 21.8159°N, 94.3542°W, and the other for a lower optical thickness (τ=4.44) cloud and latitude and longitude 24.0042°N, 92.0033°W.

data sets are the pixel-level (or level 2) retrieved cloud products discussed in detail by Platnick et al. [50]. The bi-spectral method developed by Nakajima and King [51] is implemented to infer cloud optical and microphysical properties. Cloud top height is derived from cloud top pressure (CTP) and atmospheric temperature profile data. MODIS CTP data are retrieved from bands 32–36 based on the CO_2 slicing technique [52,53]. To avoid uncertainties associated with satellite-based cloud retrievals over land, the collocated measurements by the Aqua MODIS and AIRS at 19:30 UTC, on 7 September 2009, over the Gulf of Mexico, are used in this study. Fig. 7 shows the ice cloud optical thickness of the Aqua MODIS granule.

Yang et al. [54] discussed different features of ice and water cloud BTs in the 8–13 μm atmospheric window spectral region and demonstrated that incorrectly identified cloud phase can give rise to significant errors in cloud radiance simulations. The method used for MODIS to infer cloud thermodynamic phase (ice or water) is based on an infrared bispectral algorithm [50,55]. The physical principles for discriminating water cloud from ice cloud depend on the bulk scattering properties of water droplets and ice crystals and are described in detail by Baum et al. [56]. In this study, ice cloud pixels are selected from the MODIS Quality Assurance (QA) 1-km data using QA=3 to filter out those pixels with water, mixed, or unknown phases.

Two MODIS pixels from ice clouds are selected from the granule shown in Fig. 7: one for an optically thick cloud (τ=50.73), and the second for a cloud with a lower optical thickness (τ=4.44). Comparisons between the high-spectral-resolution BTs simulated from the CRTM and those observed from an AIRS for the two selected MODIS pixels are shown in Figs. 8 and 9. Note the BT values of the AIRS bad channels have been eliminated in Figs. 8 and 9. The cloud geometric thickness is determined by the minimization method [57]. The BT differences between observations

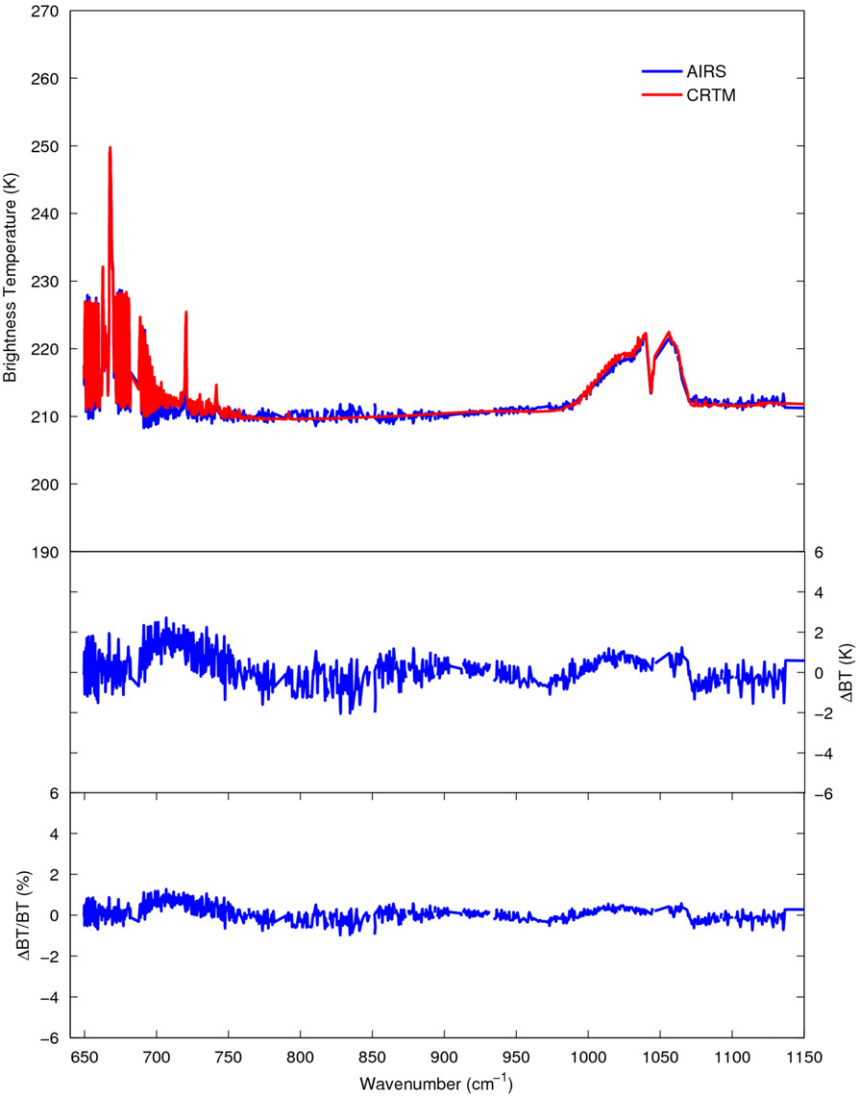

Fig. 8. Comparison between the spectral BTs simulated from the CRTM and those observed by AIRS for selected MODIS ice cloud pixels having a large optical thickness.

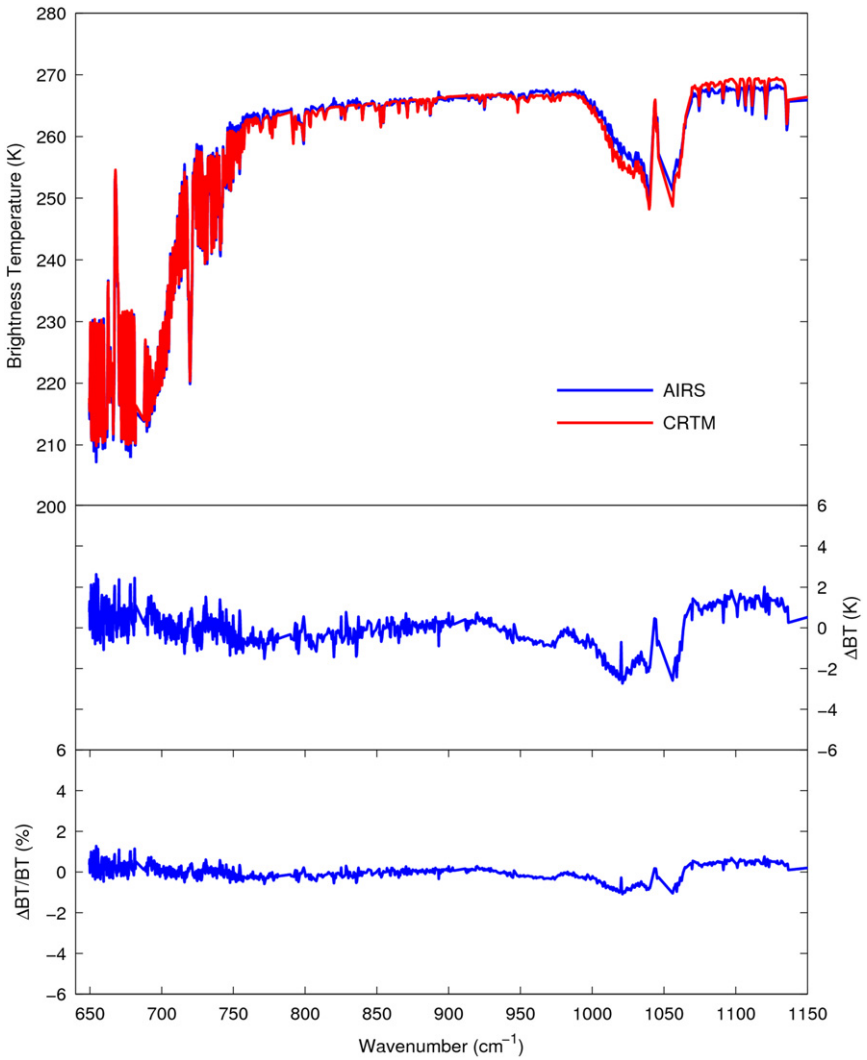

Fig. 9. Comparison between the spectral BTs simulated from the CRTM and those observed by an AIRS for selected MODIS pixels having a small optical thickness.

and simulations and the relative derivations are also shown. As evidenced from the figure, the CRTM performs well in radiance simulations.

The BT differences between the CRTM-based simulations and AIRS observations may be attributed to many sources including the uncertainties in cloud optical thickness and effective particle size, the lack of cloud base height information, and the inaccuracies in atmospheric temperature and humidity profiles. Moreover the MODIS cloud optical thickness and particle size are derived from MODIS visible and near-infrared bands, whereas the simulations are performed in the infrared spectrum. The spectral inconsistency in the cloud optical properties in the MODIS retrieval and the CRTM simulation may also be responsible for the discrepancies between the model simulations and the observations. In addition, the time of the chosen granule of MODIS and AIRS measurements is not exactly the same as the ECMWF data, and errors may be incurred in temporally interpolating the ECMWF atmospheric profiles. Thus, the response of the CRTM-based simulations to the uncertainties in the input cloud properties and atmospheric constituent profiles must be estimated.

A practical approach to estimate the effect of the uncertainties of the MODIS cloud products and ECMWF atmospheric profiles on the CRTM-based TOA BTs is the perturbation method, which perturbs the values of the input cloud properties and atmospheric parameters. For the sensitivity study, we first consider the preceding optically thin cloud case as a reference. To understand the effect of the ice effective particle radius, the uncertainties in the particle size are assumed to be the order of $\pm 5\%$, whereas the other parameters are kept the same. The variations in simulated TOA BTs associated with the perturbation of the effective particle radius are shown in Fig. 10(a) and the corresponding relative differences shown in Fig. 10(d). Likewise, the TOA radiance variations

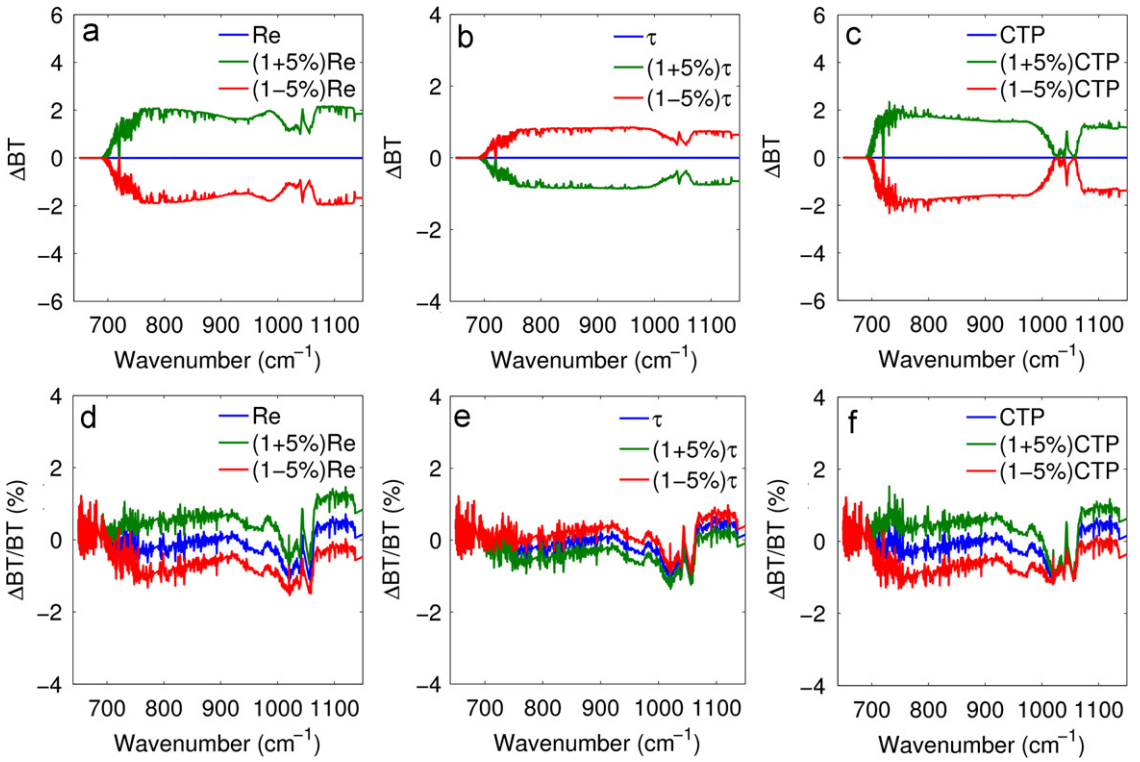

Fig. 10. The CRTM-based brightness temperature differences associated with the perturbation of the various ice cloud properties: (a) effective particle radius, (b) cloud optical thickness, and (c) cloud top pressure (CTP), in the case of optically thin cloud. Panels (d), (e), and (f) are the corresponding relative discrepancies with respect to the AIRS radiances.

associated with the perturbation in optical thickness and cloud top height are simulated and the relevant results are shown in Fig. 10(b), (c), (e), and (f).

The same method is employed to investigate the effect of the uncertainties in the input ECMWF atmospheric temperature and humidity profiles. For simplification, the temperature deviations of ± 3 K and humidity deviations of $\pm 5\%$ are assumed in all vertical layers. The effect of the temperature perturbation on the CRTM-based BTs is shown in Fig. 11(a). The corresponding relative discrepancies in comparison with the AIRS measurements are shown in Fig. 11(c). In the same way, the uncertainties associated with the humidity perturbation are examined and shown in panels (b) and (d) of Fig. 11.

From Figs. 10 and 11, it is evident that the uncertainties in the temperature profile have the largest effect on the TOA BTs at almost all AIRS channels when a ± 3 K perturbation is added. On the same order are the effects of the uncertainties in the effective particle radius and CTP, with a $\pm 5\%$ perturbation at the spectral range in the atmosphere window. The impact of the uncertainties in cloud optical thickness and the atmospheric humidity profile on the TOA BTs are much weaker than those of other input parameters on the order of ± 1 K when a $\pm 5\%$ perturbation is considered.

Similarly, the uncertainties from the input MODIS cloud products and ECMWF atmospheric profile are investigated for an optically thick cloud by using the same perturbation values for cloud parameters and the atmospheric profiles. Figs. 12 and 13 show the relevant results. In the thick cloud case, the uncertainties in the temperature profile have the largest effect on the TOA BTs at almost all AIRS channels when a ± 3 K perturbation is considered. However, the TOA BTs are not as sensitive as those in the thin cloud case, when a $\pm 5\%$ perturbation is added to the particle effective size.

The uncertainty studies show the CRTM-based simulated brightness temperatures (BTs) at the top of the atmosphere (TOA) are highly sensitive to the atmospheric temperature profile and cloud top pressure (CTP) for both optically thin and thick clouds cases. Note the validation of cloudy RTM with radiance measurements is always difficult, since no true cloud and clear-sky parameters are available. In this study, the BT differences between the CRTM calculated and the AIRS observed may attribute to various factors as mentioned previously. Ideally, collocated RAwinsonde Observation (RAOB) profiles, lidar cloud measurements, and AIRS radiance measurements should be used for CRTM validation.

6. Summary and conclusions

An assessment of the CRTM capability of simulating high spectral resolution IR radiances in comparison with spectra routinely obtained from AIRS and IASI operational sensors is reported. To evaluate the CRTM, a rigorous model

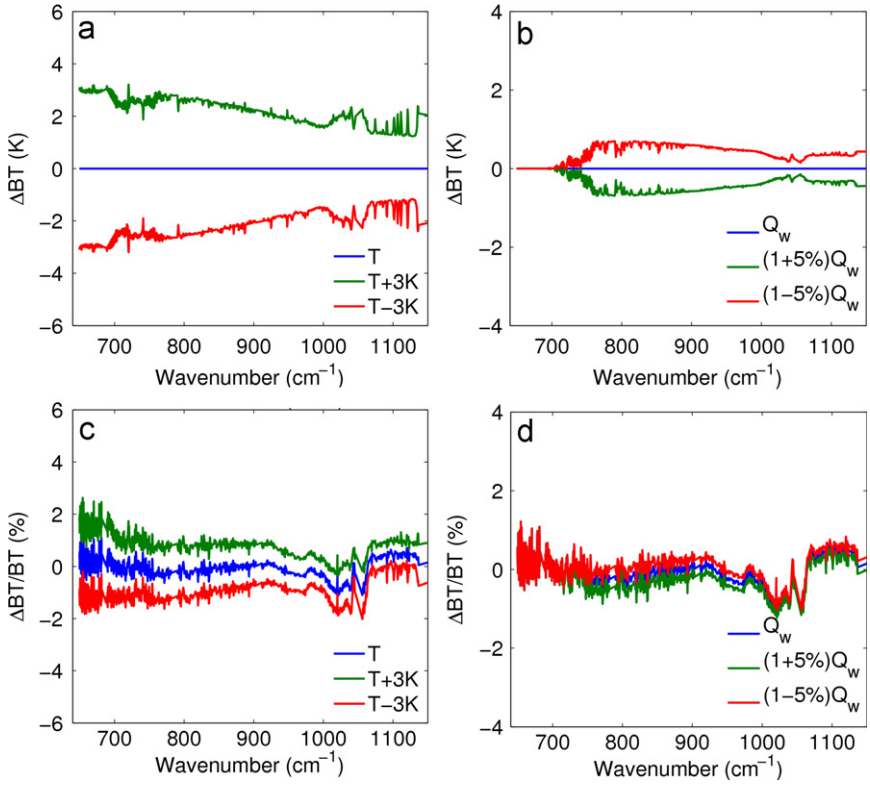

Fig. 11. The CRTM-based brightness temperature differences associated with the perturbation of (a) the atmospheric temperature, and (b) mass mixing ratio of water vapor. Panels (c) and (d) are the corresponding relative discrepancies with respect to the AIRS measurements.

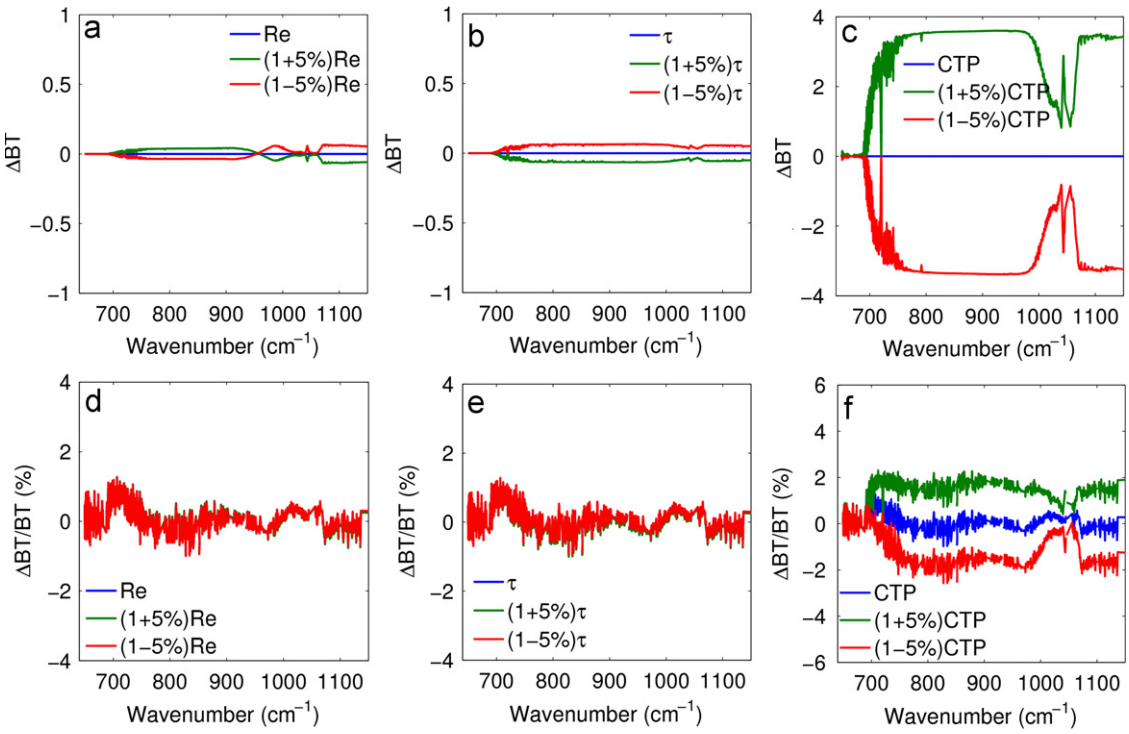

Fig. 12. Similar to Fig. 10, but for an optically thick cloud case. The properties of the reference cloud are the same as those in Fig. 8.

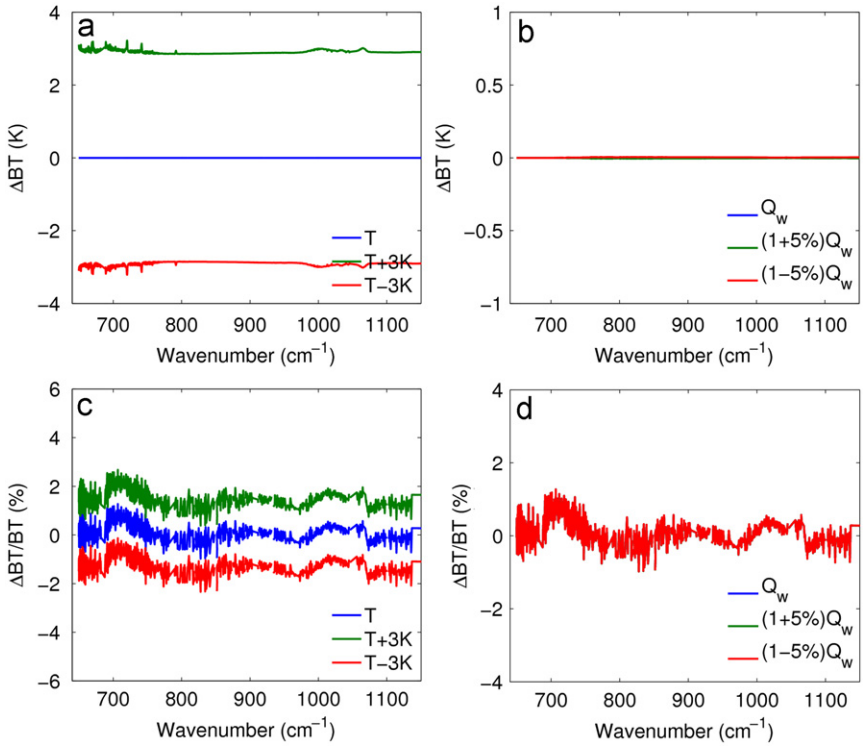

Fig. 13. Similar to Fig. 11, but for an optically thick cloud. The properties of the reference cloud are the same as those in Fig. 8.

based on a combination of the discrete ordinate radiative transfer (DISORT) model and the line-by-line radiative transfer model (LBLRTM) was used as a reference. The CRTM simulated IASI band 1 spectral BTs were compared with those from the LBLRTM+DISORT model in both clear-sky and ice cloud cases. The comparison indicates the CRTM RMS errors, below 0.2 K, except for clouds with small ice particles (De=30 μm), to be acceptable for our cases. We investigated the sensitivity of the CRTM high spectral BTs to cloud macrophysical (i.e., cloud top height and geometric thickness) and microphysical properties (IWP and particle size). A change of 1 km in the cloud top height affects the high spectral BTs approximately two times more than that of a like change in the cloud geometric thickness. Although the variation in the cloud geometric thickness has less influence on simulated upwelling BTs compared with a similar variation in cloud top height, the cloud geometric thickness is not negligible. In addition, a comparison of computational efficiency shows that the CRTM is more than two orders of magnitude faster than the DISORT.

We compared CRTM simulated BTs, having used the MODIS cloud products and ECMWF atmospheric profile as an input, with the AIRS level 1B radiance data. The results between the CRTM simulated high-spectral-resolution BTs and those observed by AIRS for two selected MODIS pixels of optically thick and thin ice cloud are reported. The CRTM appears to have performed well in these radiance simulations.

The effect of the uncertainties in the ice cloud properties and atmospheric profiles on the CRTM simulation has been examined. The results indicate, for both optically thin and thick clouds, the CRTM-based simulated brightness temperatures (BTs) at the top of the atmosphere (TOA) are highly sensitive to the perturbation of the atmospheric temperature profile and cloud top pressure (CTP). For an optically thick cloud, the CRTM-based BTs are not sensitive to the uncertainties in the effective particle size, optical thickness, and the humidity profile. However, for an optically thin cloud, the simulated TOA BTs are sensitive to the uncertainties in the effective particle size and optical thickness.

Acknowledgments

This study is partly supported by the National Oceanic and Atmospheric Administration (DG133E09CN0258). Bryan Baum is supported through NASA Grant NNX08AF81G.

References

[1] Errico RM, Ohring G, Bauer P, et al. Assimilation of Satellite Cloud and Precipitation Observations in Numerical Weather Prediction Models: introduction to the JAS Special Collection. J Atmos Sci 2007;64:3737–41.

[2] Greenwald TJ, Hertenstein R, Vukicevic T. An all-weather observational operator for radiance data assimilation with mesoscale forecast models. Mon Weather Rev 2002;130:1882–97, doi:10.1175/1520-0493(2002)130;<1882:AAWOOF>2.0.CO;2.

[3] Greenwald TJ, Bennartz R, O'Dell C, et al. Fast computation of microwave radiances for data assimilation using the "Successive

Order of Scattering" method. J Appl Meteorol 2005;44:960–6, doi:10.1175/JAM2239.1.
[4] Anderson E, Bauer P, Beljaars A, et al. Assimilation and modeling of the atmospheric hydrological cycle in the ECMWF forecasting system. Bull Am Meteorol Soc 2005;86:387–402, doi:10.1175/BAMS-86-3-387.
[5] Weng F. Advances in radiative transfer modeling in support of satellite data assimilation. J Atmos Sci 2007;64(3799-3807)10.1175/2007JAS2112.1.
[6] Weng F, Zhu T, Yan B. Satellite data assimilation in numerical weather prediction models. Part II: uses of rain-affected radiances from microwave observations for hurricane vortex analysis. J Atmos Sci 2007;64:3910–25, doi:10.1175/2006JAS2051.1.
[7] Han Y, van Delst P, Liu Q, et al. Community radiative transfer model (CRTM): Version 1, NOAA Technical Report. NOAA, Washington, DC; 2006; 122 pp.
[8] Liu Q, Liang X, Han Y, et al. Effect of out-of-band response in NOAA-16 AVHRR channel 3b on top-of-atmosphere radiances calculated with the community radiative transfer model. J Atmos Oceanic Technol 2009;26:1968–72.
[9] Aumann HH, Chahine MT, Gautier C, et al. AIRS/AMSU/HSB on the aqua mission: desing, science objectives, data products, and processing systems. IEEE Trans Geosci Remote Sensing 2003;41:252–64.
[10] Chalon G, Cayla FR, Diebel D. IASI: an advance sounder for operational meteorology. IAF 2001 conference proceedings. 2001.
[11] Weisz E, Huang H, Li J, et al. International MODIS/AIRS processing package: AIRS applications and products. J Am Rocket Soc 2007;1:1–23.
[12] Li J, Liu H. Improved hurricane track and intensity forecast using single field-of-view advanced IR sounding measurements. Geophys Res Lett 2009;36:L11813, doi:10.1029/2009GL038285.
[13] Schmit TJ, Li J, Ackerman SA, et al. High spectral and high temporal resolution infrared measurements from geostationary orbit. J Atmos Oceanic Technol 2009;26:2273–92.
[14] Clough SA, Iacono MJ, Moncet JL. Line-by-line calculation of atmospheric fluxes and cooling rates: application to water vapor. J Geophys Res 1992;97:15761–85.
[15] Stamnes K, Tsay SC, Wiscombe W, et al. Numerically stable algorithm for discrete-ordinate-method radiative transfer in multiple scattering and emitting layered media. Appl Opt 1988;27:2502–9.
[16] Liu Q, Weng F. Advanced doubling–adding method for radiative transfer in planetary atmosphere. J Atmos Sci 2006;63:3459–65.
[17] Clough SA, Shephard MW, Mlawer EJ, et al. Atmospheric radiative transfer modeling: a summary of the AER codes, short communication. J Quant Spectrosc Radiat Transfer 2005;91:233–44.
[18] Moncet JL, Uymin G, Lipton AE, et al. Infrared radiance modeling by optimal spectral sampling. J Atmos Sci 2008;65:3917–34, doi:10.1175/2008JAS2711.1.
[19] Chandrasekhar S. In: Radiative transfer. New York: Dover; 1960.
[20] Berk A, Bernstein L, Anderson GP, et al. MODTRAN cloud and multiple scattering upgrades with application to AVIRIS. Remote Sensing Environ 1998;65:367–75.
[21] Richiazzi P, Yang S, Gautier C, et al. SBDART: A research and teaching software tool for plane-parallel radiative transfer in the Earth's atmosphere. Bull Am Meteorol Soc 1998;79:2101–14.
[22] Wiscombe WJ. The delta-M method: rapid yet accurate radiative flux calculations for strongly asymmetric phase functions. J Atmos Sci 1977;34:1408–22.
[23] Hu YX, Wielicki B, Lin B, et al. δ-Fit: a fast and accurate treatment of particle scattering phase functions with weighted singular-value decomposition least-squares fitting. J Quant Spectrosc Radiat Transfer 2000;65:681–90.
[24] Ding S, Xie Y, Yang P, et al. Estimate of radiation over clouds and dust aerosols: optimized number of terms in phase function expansion. 2009;110:1190–8.
[25] Liou KN. In: An introduction to atmospheric radiation. 2nd ed.. San Diego, CA: Academic Press; 2002.
[26] Yang P, Liou KN. Finite-difference time domain method for light scattering by small ice crystals in three-dimensional space. J Opt Soc Am 1996;A13:2072–85.
[27] Yang P, Liou KN. Geometric-optics-integral-equation method for light scattering by nonspherical ice crystals. Appl Opt 1996;35:6568–84.
[28] Yang P, Wei H, Huang H, et al. Scattering and absorption property database for nonspherical ice particles in the near–through far-infrared spectral region. Appl Opt 2005;44:5512–23.
[29] Baum BA, Heymsfield A, Yang P, et al. Bulk scattering properties for the remote sensing of ice clouds I: microphysical data and models. J Appl Meteorol 2005;44:1885–95.
[30] Baum BA, Yang P, Heymsfield AJ, et al. Bulk scattering properties for the remote sensing of ice clouds II: narrowband models. J Appl Meteorol 2005;44:1896–911.
[31] Baum BA, Yang P, Nasiri S, et al. Bulk scattering properties for the remote sensing of ice clouds. III: high resolution spectral models from 100 to 3250 cm^{-1}. J Appl Meteorol Climatol 2007;46:423–34.
[32] King MD, Platnick S, Yang P, et al. Remote sensing of liquid water and ice cloud optical thickness and effective radius in the arctic: application of airborne multispectral MAS data. J Atmos Oceanic Technol 2004;21:857–75.
[33] King MD, Platnick S, Hubanks PA, et al. Collection 005 change summary for the MODIS cloud optical property (06_OD) algorithm. MODIS Collection 005 Change Summary Document. 2006. 23 p.
[34] Nakajima T, King MD. Determination of the optical thickness and effective particle radius of clouds from reflected solar radiation measurements. Part I: theory. J Atmos Sci 1990;47:1878–93.
[35] King MD, Tsay SC, Plantick SE, et al. Cloud retrieval algorithms for MODIS: optical thickness, effective particle radius, and thermodynamic phase. MODIS algorithm theoretical basis document, No. ATBD-MOD-05. 1997.
[36] Rolland P, Liou KN, King MD, et al. Remote sensing of optical and microphysical properties of cirrus clouds using MODIS channels: methodology and sensitivity to physical assumptions. J Geophys Res 2000;105:11721–38.
[37] Hong G, Yang P, Huang H, et al. The sensitivity of ice cloud optical and microphysical passive satellite retrievals to cloud geometrical thickness. IEEE Trans Geosci Remote Sensing 2007;45:1315–23.
[38] Wei H, Yang P, Li J, Baum BA, et al. Retrieval of ice cloud optical thickness from atmospheric infrared sounder (AIRS) measurements. IEEE Trans Geosci Remote Sensing 2004;42:2254–65.
[39] Huang H, Yang P, Wei H, et al. Inference of ice cloud properties from high-spectral resolution infrared observations. IEEE Trans Geosci Remote Sensing 2004;42:842–52.
[40] McClatchey RA, Fenn RW, Selby JE, et al. Optical properties of the atmosphere. AFCRL Environmental Research Paper no. 411 (3rd ed.). 1972.
[41] Niu J, Yang P, Huang H, et al. A fast infrared radiative transfer model for overlapping clouds. J Quant Spectrosc Radiat Transfer 2007;103:447–59.
[42] Zhang Z, Yang P, Kattawar GW, et al. A fast infrared radiative transfer model based on the adding–doubling method for hyperspectral remote sensing applications. J Quant Spectrosc Radiat Transfer 2007;105:243–63.
[43] Blumstein D, Chalon G, Carlier T, et al. IASI instrument: technical overview and measured performances. SPIE 2004-5543-22. 2004.
[44] Gaiser SL, Aumann HH, Strow LL, et al. In-flight spectral calibration of the atmospheric infrared sounder. IEEE Trans Geosci Remote Sensing 2003;41:287–97.
[45] Li J, Menzel WP, Sun F, Schmit TJ, et al. AIRS subpixel cloud characterization using MODIS cloud products. J Appl Meteorol 2004;43:1083–94.
[46] Li J, Menzel WP, Zhang W, et al. Synergistic use of MODIS and AIRS in a variational retrieval of cloud parameters. J Appl Meteorol 2004;43:1619–34.
[47] Ham SH, Sohn BJ, Yang P, et al. Assessment of the quality of MODIS cloud products from radiance simulations. J Appl Meteorol Climatol 2009;48:1591–611.
[48] Kahn BH, Fishbein E, Nasiri SL, et al. The radiative consistency of atmospheric infrared sounder and moderate resolution imaging spectroradiometer cloud retrievals. J Geophys Res 2007;112:D09201, doi:10.1029/2006JD007486.
[49] King MD, Menzel WP, Kaufman YJ, et al. Cloud and aerosol properties, precipitable water, and profiles of temperature and humidity from MODIS. IEEE Trans Geosci Remote Sensing 2003;41(2):442–58.
[50] Platnick S, King MD, Ackerman SA, et al. The MODIS cloud products: algorithms and examples from Terra. IEEE Trans Geosci Remote Sensing 2003;41(2):459–73.
[51] Nakajima T, King MD. Determination of the optical thickness and effective particle radius of clouds from reflected solar radiation measurements. Part I: theory. J Atmos Sci 1990;47:1878–93.
[52] Ackerman SA, Smith WL, Spinhirne JD, et al. The 27–28 October 1986 FIRE IFO cirrus case study: spectral properties of cirrus clouds in the 8–12 μm window. Mon Weather Rev 1990;118:2377–88.
[53] Strabala KI, Ackerman SA, Menzel WP. Cloud properties inferred from 8 to 12 μm data. J Appl Meteorol 1994;2:212–29.

[54] Yang P, Wei H, Baum BA, et al. The spectral signature of mixed-phase clouds composed of nonspherical ice crystals and spherical liquid droplets in the terrestrial window region. J Quant Spectrosc Radiat Transfer 2003;79–80:1171–88.
[55] Menzel WP, Frey R, Zhang H, et al. MODIS global cloud-top pressure and amount estimation: algorithm description and results. J Appl Meteorol Climatol 2008;47:1175–98.
[56] Baum BA, Kratz DP, Yang P, et al. Remote sensing of cloud properties using MODIS airborne simulator imagery during SUCCESS. I. Data and models. J Geophys Res 2000;105(11): 767–80.
[57] Yue Q, Liou KN. Cirrus cloud optical and microphysical properties determined from AIRS infrared spectra. Geophys Res Lett 2009;36: L05810.